Akademie věd
České republiky

Teze disertace

k získání vědeckého titulu "doktor věd"

ve skupině věd ……Technické vědy……

Mechanical Properties of Advanced Metallic Materials Studied by Laser-Ultrasonic Methods

……

název disertace

Komise pro obhajoby doktorských disertací v oboru ……Aplikovaná a teoretická mechanika……

Jméno uchazeče ……doc. Ing. Hanuš SEINER, Ph.D.……

Pracoviště uchazeče ……..Ústav termomechaniky AV ČR, v.v.i.

Místo a datum ……..Praha, 10. 7. 2020……..

Résumé of the Dissertation

The dissertation *Mechanical Properties of Advanced Metallic Materials Studied by Laser-Ultrasonic Methods* gives a comprehensive summary of the research carried out in the field of laser-ultrasonic (LU) characterization of mechanical properties materials by the applicant or under the applicant's supervision. The main aim of the dissertation is to show how these methods, based on elastic wave propagation and vibrations in the ultrasonic frequency range, can be utilized for materials characterization, pointing out the advantages of using lasers for generation and detection of ultrasound instead of more conventional techniques (e.g., instead of using piezoelectric transducers).

The dissertation consists of two parts. The first part (Chapter 1) is introductory, giving a description of experimental devices for LU characterization developed and operated at the Institute of Thermomechanics, Czech Academy of Sciences, that were used for the research reported in the thesis. This first part also summarizes the contribution of the applicant's students to the reported research and briefly describes the applicant's research activities outside the topic of the thesis. The second part (Chapters 2, 3, 4 and 5) consists of twelve commented research papers illustrating the versatility of the used LU approaches and their ability to contribute significantly to characterization of advanced metallic materials. For the shape memory alloys (Chapter 2), it is shown that the LU approaches can provide a valuable information on both temperature-induced and stress induced changes of shear elastic coefficients indicating the instability of the crystal lattice. Similarly, the lattice instability due to magnetostriction is studied for materials with strong magnetoelastic coupling (Chapter 3). For materials undergoing diffusive phase transition (Chapter 4), the LU methods are shown to be able to detect transitions in very small volume factions of materials, based on the changes of macro-scale mechanical properties. Finally, Chapter 5 proves the LU methods very efficient for studying ultrafine-grained materials and elucidating the role the grain boundaries play in the mechanics and micro-mechanics of these materials.

The below given extended synopsis of the dissertation includes the description of the LU experimental methods utilized for the reported research, as well as a summary of the main results of their applications to a broad range of advance metallic materials.

1 Introduction

Understanding the relationship between the elastic constants and elastic wave propagation in an anisotropic solid dates back to the 19th century, when the most fundamental theoretical background was developed by Christoffel [1]. During the following decades, the solutions to the so-called *Christoffel's equation* were utilized either for predicting the speed of elastic wave propagation in known materials, or, inversely, for determining some of the elastic constants of unknown materials by elastic (ultrasonic) wave speed measurements (see the textbooks [2, 3, 4] and the historical references therein). However, it took more than a century until the computational power enabled the inverse problem to be solved *completely*, i.e., having an extensive set of wave velocity data for various material direction as an input, and providing a complete tensor of elastic constants of an anisotropic material with lower symmetry than cubic as an output of the calculation. A remarkable result was achieved by Francois et al.[5], who used elastic wave velocity data for 13 unique propagation directions on a polyhedral sample to determine all 21 independent elastic constants of a generally anisotropic solid. This experiment proved that the elastic response of a material of any symmetry can be fully characterized by ultrasonic methods, a goal that is nearly impossible to reach by any other tool of experimental mechanics.

Among the improvements the ultrasonic methods underwent since the times of Christoffel, one can be seen as the most seminal: the use of lasers [6, 7, 8, 9, 10]. Focused laser beams are capable of both generating and detecting the ultrasonic waves in solids, and their employment brings significant advantages. For example, the propagation direction (i.e. the direction from the source to the receiving point) can be set just by positioning the pump beam and the probe beam over the surfaces of the sample; or, thanks to their non-contact nature, laser-based ultrasonic measurements can be easily performed under extreme conditions, such at high temperatures [11, 12] or even at high hydrostatic pressures [13, 14]. At the same time, the incredible versatility of laser-based generation of ultrasound can be utilized. Just as a result of using proper optics, the thermoacoustic sources arising from an impact of a focused laser beam on the surface of the sample can take forms of points, lines or periodic patterns. Similarly, the temporal characteristic of the source can range from extremely short pulses (generating broadband ultrasonic waves and enabling to reach up to GHz frequency range) to narrowband generation due to temporal modulation [10, 15, 16, 17, 18].

All these features enabled laser-ultrasonic (LU) methods to get established as a new and rapidly developing branch of experimental mechanics in the past few decades. Originating from the pioneering works in 1960s [19, 20, 21, 22], the LU approaches can be nowadays found used as reliable tools for materials characterization in a broad range of research areas, including biomechanics [23, 24, 25], geology [26, 27], metal processing [28, 29] and nanotechnology [30, 31]. Several new experimental arrangement utilizing these approaches have been developed, ranging from the rather classical point-source/point-receiver [32, 33] setups to transient grating spectroscopy [34, 35, 36] or picosecond ultrasonics [15, 16]. In 2015, the achievement by Francois et al. [5] was repeated by Sedlák et al. [37] using the laser-based resonant ultrasound spectroscopy method: again, all 21 elastic constants of a generally anisotropic material were determined, but this time using just one small, simply shaped sample, and with a significantly smaller experimental uncertainty. In other words, the emergence of laser made the ultrasonic measurements much more directly available to the materials science.

The DSc. dissertation entitled *Mechanical Properties of Advanced Metallic Materials Studied by Laser-Ultrasonic Methods* summarizes the results of LU measurement performed on a broad range of advanced metallic materials by the applicant or under the applicant's supervision in case that the measurements were done by his graduate students. By giving such a summary, the dissertation aims to point out how significantly the application of LU methods can contribute to the progress in the given field. In this sense, while the scope of the dissertation is pretty narrow from the point of view of experimental mechanics, it is relatively diverse from the point of view of materials science. The dissertation does not have any ambition to contribute to the topic of the development of the LU methods themselves as far as the principles, instrumentation or signal processing are concerned. Instead, it aims to explore how the results of the LU methods can elucidate several problems from the field of mechanics of materials.

The results included in the dissertation are limited to metallic materials (pure metals, alloys and metal-metal composites). Metals are particularly suitable for LU characterization, as they posses a good combination of thermal conductivity and thermal expansion for thermoacoustic generation of ultrasonic waves, and, at the same time, can be mirror-polished to get maximum reflectivity for the probe beam. On the other hand, unlike in ceramics or in dielectrics in general, the propagation of ultrasonic waves in metals can be strongly atten-

tuated by several different internal friction mechanisms, including dislocation damping, magnetoelastic damping or grain boundary sliding [38]. This brings several challenges for the LU characterization, but, simultaneously, enables the LU methods to bring a deeper insight into these mechanisms, their temperature evolutions, etc.. From this point of view, this dissertation covers a broader range of approaches to LU characterization of metals; besides the determination of the elastic constants themselves, it discusses also their relation to the internal friction parameters, often trying to achieve a more complete picture of the processes in the given material based on the interplay of both parameters. This diversity of approaches, again, aims to illustrate the versatility and power of the described methods.

The dissertation is composed of twelve research papers, covering results of LU measurements on four diverse (but related) groups of materials. Each group is first introduced by a short subsection, explaining mainly the reasons for applications of the LU methods for such materials, but also giving a brief introduction into the related materials science problems, including the basic terminology and state-of-the art. Each paper is then commented in terms of the applicant's personal contribution and the collaboration with other research groups.

The included papers are[1]:

A1 – Thomasová, M., Sedlák, P., Seiner, H., Janovská, M., Kabla, M., Shilo, D., Landa, M. Young's moduli of sputter-deposited NiTi films determined by resonant ultrasound spectroscopy: Austenite, R-phase, and martensite (2015) Scripta Materialia, 101, pp. 24-27. (IF= 5.079, 26 citations. The applicant was the corresponding author, the first author was his graduate student.)

A2 – Thomasová, M., Seiner, H., Sedlák, P., Frost, M., Ševčík, M., Szurman, I., Kocich, R., Drahokoupil, J., Šittner, P., Landa, M. Evolution of macroscopic elastic moduli of martensitic polycrystalline NiTi and NiTiCu shape memory alloys with pseudoplastic straining (2017) Acta Materialia, 123, pp. 146-156. (IF=7.656, 23 citations. The applicant was the corresponding author, the first author was his graduate student.)

A3 – Seiner, H., Stoklasová, P., Sedlák, P., Ševčík, M., Janovská, M., Landa, M., Fukuda, T., Yamaguchi, T., Kakeshita, T. Evolution of soft-phonon modes in Fe-Pd shape memory alloy under large elastic-like strains (2016) Acta Materialia, 105, pp. 182-188. (IF=7.656, 11 citations. The applicant was both the corresponding author and the first author.)

[1]The impact factors and citation counts are relevant to July 10, 2020. The citation counts are taken from the SCOPUS database.

B1 – <u>Seiner, H.</u>**, Heczko, O., Sedlák, P., Bodnárová, L., Novotný, M., Kopeček, J., Landa, M. Combined effect of structural softening and magneto-elastic coupling on elastic coefficients of NiMnGa austenite (2013) Journal of Alloys and Compounds, 577 (SUPPL. 1), pp. S131-S135.** (IF=4.650, 21 citations. The applicant was the first author.)

B2 – <u>Seiner, H.</u>**, Sedlák, P., Bodnárová, L., Drahokoupil, J., Kopecký, V., Kopeček, J., Landa, M., Heczko, O. The effect of antiphase boundaries on the elastic properties of Ni-Mn-Ga austenite and premartensite (2013) Journal of Physics Condensed Matter, 25 (42), art. no. 425402.** (IF=2.707, 16 citations. The applicant was both the corresponding author and the first author.)

B3 – <u>Seiner, H.</u>**, Kopeček, J., Sedlák, P., Bodnárová, L., Landa, M., Sedmák, P., Heczko, O. Microstructure, martensitic transformation and anomalies in c'-softening in Co-Ni-Al ferromagnetic shape memory alloys (2013) Acta Materialia, 61 (15), pp. 5869-5876.** (IF=7.656, 16 citations. The applicant was the first author.)

C1 – **Nejezchlebová, J.,** <u>Seiner, H.</u>**, Ševčík, M., Landa, M., Karlík, M. Ultrasonic detection of ductile-to-brittle transitions in free-cutting aluminum alloys (2015) NDT and E International, 69, pp. 40-47.** (IF=3.461, 4 citations. The applicant was the corresponding author, the first author was his graduate student.)

C2 – **Nejezchlebová, J., Janovská, M.,** <u>Seiner, H.</u>**, Sedlák, P., Landa, M., Šmilauerová, J., Stráský, J., Harcuba, P., Janeček, M. The effect of athermal and isothermal ω phase particles on elasticity of $\beta-$Ti single crystals (2016) Acta Materialia, 110, pp. 185-191.** (IF=7.656, 22 citations. The applicant was the corresponding author, the first author was his graduate student.)

C3 – **Nejezchlebová, J., Janovská, M., Sedlák, P., Šmilauerová, J., Stráský, J., Janeček, M.,** <u>Seiner, H.</u> **Elastic constants of β-Ti15Mo (2019) Journal of Alloys and Compounds, 792, pp. 960-967.** (IF=4.650, 2 citations. The applicant's graduate student was both the first author and the corresponding author. The applicant was the last author (denoting the group leader).)

D1 – <u>Seiner, H.</u>**, Bodnárová, L., Sedlák, P., Janeček, M., Srba, O., Král, R., Landa, M. Application of ultrasonic methods to determine elastic anisotropy of polycrystalline copper processed by equal-channel angular pressing (2010) Acta Materialia, 58 (1), pp. 235-247.** (IF=7.656, 30 citations. The applicant was both the corresponding author and the first author.)

D2 – **Koller, M., Sedlák, P.,** <u>Seiner, H.</u>**, Ševčík, M., Landa, M., Stráská, J., Janeček, M. An ultrasonic internal friction study of ultrafine-grained AZ31 magnesium alloy (2014) Journal of Materials Science, 50 (2), pp. 808-818.** (IF=3.553, 10 citations. The applicant was the corresponding author, the first author was his graduate student.)

D3 – Seiner, H., Cizek, J., Sedlák, P., Huang, R., Cupera, J., Dlouhy, I., Landa, M. Elastic moduli and elastic anisotropy of cold sprayed metallic coatings (2016) Surface and Coatings Technology, 291, pp. 342-347. (IF=3.784, 13 citations. The applicant was the first author.)

These papers bring a representative, yet not exhaustive summary of the applicant's work in the field of LU-characterization of metallic materials. Several papers from this research area are not included, either because the applicant's contribution (or the contribution of his students) was not major, or because these papers are rather of technical nature, reporting on rather incremental research, or being not published in sufficiently high-ranking journals. Also paper older than from 2010 were not considered for inclusion in the dissertation.

2 LU experimental arrangements utilized for the reported research

2.1 Modal resonant ultrasound spectroscopy for characterization of elastic anisotropy

The resonant ultrasound spectroscopy (RUS,[39, 40]) method is one of the most accurate experimental techniques for determination of elastic constants of solids, particularly suitable for anisotropic materials. The reason originates from the resonant nature of this method – RUS is based on measuring resonant spectra of free elastic vibrations (i.e., steady ultrasonic waves) of a small sample of the examined solid. Even very small changes of the elastic constants of the material are reflected by measurable changes of the resonant frequencies, especially as regards the shear elastic constants, since the lowest resonant modes are typically related to pure shears. That makes RUS an irreplaceable tool for characterization of soft shearing modes in materials.

The basic principles of RUS are described in the pioneering works [39, 40] and elaborated in more detail in [37]. Here, we summarize just the main ideas:

The resonant frequencies and resonant modes can be understood as stationary points of the Lagrangian energy Λ of the sample. Hence, by solving numerically the equation

$$\delta\Lambda\left(\mathbf{u}(\mathbf{x},t), d_i, \rho, C_{ijkl}\right) = 0 \tag{1}$$

for time-harmonic displacement fields $\mathbf{u}(\mathbf{x},t)$, where d_i are dimensions of the sample, ρ is the mass density, and C_{ijkl} is the tensor of elastic constants, and

assuming that the sample is homogeneous in both C_{ijkl} and ρ, one obtains a set of resonant (angular) frequencies ω_n ($n = 1, 2, \ldots$) and corresponding modal shapes for given dimensions, density, and guessed elastic constants. The RUS measurement provides this set experimentally. Then, in line with classical inverse approaches in acoustics, the elastic constants can be determined by minimizing an objective function

$$F(C_{ijkl}) = \sum_{n=1}^{N} \left[\omega_n^{\mathrm{calc}}(C_{ijkl}) - \omega_n^{\mathrm{exp}}\right]^2, \tag{2}$$

where N is the number of experimentally detected resonances, and the superscripts calc and exp denote the calculated and experimentally determined resonant frequencies, respectively.

In addition to the elastic constants, the RUS method also provides a valuable information on internal friction in the examined material. From widths of the individual resonant peaks, the mode-specific internal friction parameter

$$Q_n^{-1} = \frac{2\pi \mathrm{FWHM}_n}{\omega_n} \tag{3}$$

can be directly calculated, where FWHM_n stands for the full-width at half-maximum of the peak. In principle, Q_n^{-1} is dependent on the modal shape (this is essential for strongly anisotropic materials [41]), and can be also frequency dependent, especially for materials with relaxation damping [D2]. Nevertheless, for monitoring the temperature-induced changes of internal friction (or for comparing different materials as done in [D3]), average Q_n^{-1} of few dominant peaks is typically considered as a physical parameter sufficiently describing the behavior of the material.

The utilization of lasers in RUS is twofold. Firstly, the lasers can be used for detection of the vibrations, which, besides all advantages following from the non-contact nature of such a detection, allows identification of the individual vibrational modes, provided that the probe laser beam scans the surface of the sample during the measurement. This improvement was first suggested by Ogi et al.[42], who showed that the correct mode identification (i.e. the pairing between the measured resonant peaks and the shapes of vibrations) may be essential for reliable construction of the objective function (2).

Secondly, a focused laser beam can be also used for generation of the vibrations, which was first suggested by Zadler et al. [10]. This brings two main advantages: i) the sample has not to be in a direct contact with any piezoelectric

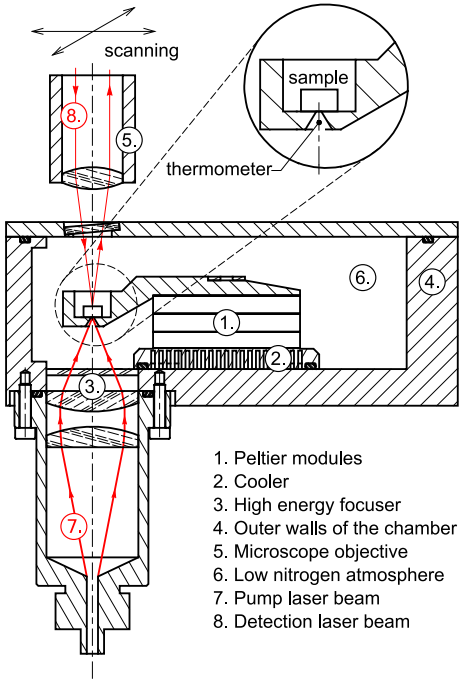

Figure 1: Schematic sketch of the temperature chamber used for the modal RUS measurements

transducer, and its vibrations are, thus, closer to real free vibrations (avoiding the clamping force from the transducers, as well as the friction between the sample and the transducer) and ii) a short laser pulse works as a very strong broadband pulse, generating a large number of vibrational modes at the same time, and thus, the RUS spectrum is recorded in a much shorter time (typically in several milliseconds) then by sweeping through the same frequency range using a transducer.

The modal[2] RUS experimental arrangement at IT-CAS exploits all of the above described features of laser-based generation and detection. It is com-

[2]Here we use the term *modal* to point out that this arrangement is capable of scanning the sample and determining the modal shapes. In other words, we use this term to distinguish this arrangement from the one described in the next subsection.

posed of a Nd:YAG laser (nominal wavelength 1.064 μm, pulse duration 8 ns, pulse energy 25 mJ; Quantel ULTRA, US) used for generation of vibrations, and a Micro System Analyser MSA500/600 (Polytec, Germany) including a scanning laser interferometer for detection of vibrations and scanning of the modal shapes. The sample itself is placed in an in-house-built vacuum chamber (see Figure 1 for a scheme and Figure 2 for a photograph), in which the temperature is controlled by a computer-driven cascade of Peltier cells. The outer walls of the chamber are cooled by a closed loop liquid cooled, acting as a heat sink for the excess heat from the Peltier cells. During the measurement, the chamber is filled with a dilute ($\sim$ 20 mbar) dry nitrogen atmosphere, which ensures a thermal contact between the sample and a cylindrical container surrounding the sample from three sides. The container is made of copper and is directly thermally connected to the active area of the Peltier cascade. It is open from above to enable the access of the scanning probe laser beam; from the bottom side, the pulse laser beam comes through a conical hole and is focused onto the bottom face of the sample. To ensure close approximation of the free vibrations, the bottom surface of the container, on which the sample is freely laid, is roughly machined. As seen from the benchmark examples [37], up to 80 modes measured using this experimental setup can match theoretically calculated frequencies with an error less than 0.1 %, which is the level of accuracy of the dimensions and density of the sample. This means that if there is any violation of the free boundary conditions from the contact between sample and the container, its effect is below the resolution limit of the method.

The Peltier cascade enables a temperature control with accuracy down to $\pm$0.01 K, whereto the temperature is measured on the sample container very close to the sample (see Figure 1). Before each measurement, a stabilization time of at least 90 seconds is used to ensure equal temperatures of the container and at the sample. Then, the measurement is performed with the probe laser beam scanning the upper surface of the sample in a regular grid, typically including from 20$\times$20 to 40$\times$40 measurement points, using between 5 and 50 complex signals averagings for each point. Depending on the number of points and the averaging, one measurement takes between 20 and 120 mins. The current setup enables measurements from $\sim$ 220 K to $\sim$ 400 K.

The resonant spectra are typically recorded in a frequency range from 50 kHz to 2 (or 3) MHz. While the instrumentation allows measurements up to 25 MHz, this is not used for most of the samples, as no peaks at such high frequencies can be usually detected due to damping. The recorded spectra are afterwards processed by a numerical software (a MATLAB toolbox developed at

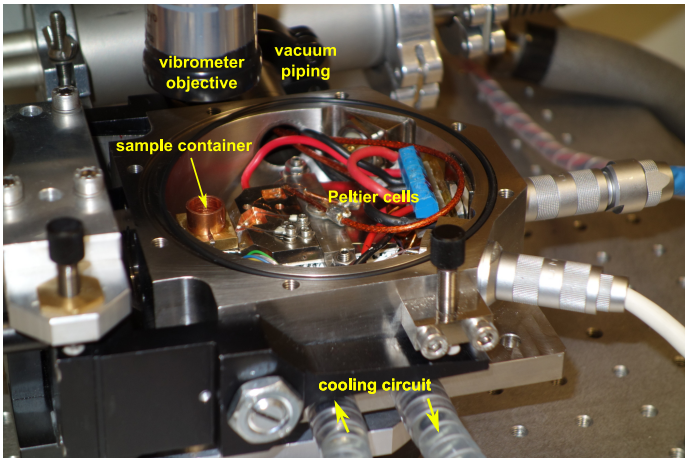

Figure 2: Detail of the temperature chamber for modal RUS measurements. Photograph by J. Zídek.

IT-CAS by P. Sedlák) in order to get the elastic constants and internal friction parameters. The software is also capable of estimating the experimental error (based on the sensitivity analysis described in detail in [37]) and to evaluate the temperature changes of the elastic constants, using a perturbation theory-based approach introduced in [43].

From the papers included in the dissertation, the above described RUS setup was used as the main experimental tool in [A1, A2, B1, B2, B3, C2, D1, D3]. It was, however, also used in the rest of them (i.e. [A3, C1, C3, D2]) for preliminary room temperature characterization of the examined materials and the identification of modal shapes (as explained in the next subsection). Besides, this arrangement was applied by the applicant and his coworkers for ultrasonic characterization of a broad variety of other materials, ranging from nanoporous semiconductors [44] to micro-architectured ceramics[45].

2.2 Single-point resonant ultrasound spectroscopy for characterization of materials at elevated temperatures

The temperature range of the modal RUS arrangement described in the previous subsection is limited from above to $\sim$ 400 K by the performance of the

Peltier cells. However, several technologically important processes in metals, such as annealing or ageing, take place at much higher temperatures [46]. In order to enable monitoring of these processes by RUS measurement, a high-temperature modification of the RUS apparatus has been designed. One of the requirements on such device was that the measurements at elevated temperature should be possible for extensive time-periods, as the annealing and ageing processes typically take hours, days or even weeks. Hence, the device was designed to be able to operate in such a regime. This required some simplifications of the experimental arrangement compared to the setup described in the previous subsection. Most importantly, the elastic response is detected just in one point at the surface of the sample, i.e. without scanning. Consequently, the probe beam is focused onto the surface of the sample directly from the interferometer head, without passing through any optical microscope or objective positioned close to the sample. This has two advantages: i) the sensitive optics can be moved further away (i.e. to a 'safe distance') from the chamber that operates at high temperatures, ii) smaller amounts of data are collected in each measurement, which is less demanding on data storage for long-term annealing/ageing experiments.

On other hand, the disadvantages of such a simplification are obvious. The modal shapes are not available, and thus, the reliable pairing of ω^{exp} with ω^{calc} is not possible. In addition, there can be always some modes that have antinodes (or small relative amplitudes) in the chosen measurement point and do not, therefore, appear in the recorded spectrum. To overcome this disadvantage, the measurements using the single-point setup must be always complemented by room-temperature scanning measurements using the device described in subsection 2.1, usually one done before the high-temperature measurements and one done after them. The first scanning measurement provides modal shapes to individual resonant peaks that can be then traced in the spectrum with increasing temperature. Similarly, the modes identified in the scanning measurement after the high-temperature measurements enables backward tracking of the modes. Of course, such an approach requires the changes of elastic constants and internal friction parameters at high temperatures to be smooth and gradual, as the resonant peaks could not be traced over sharp, discontinuous changes in the spectrum. However, the diffusion-driven ageing/annealing processes discussed in [C1, C3, D2] are typically slow and gradual, and thus, this approach is fully justified for them.

The high-temperature RUS device is depicted in Figure 3. It consists of a pulse laser Litron Nano S (nominal wavelength 1.064 μm, pulse duration 6

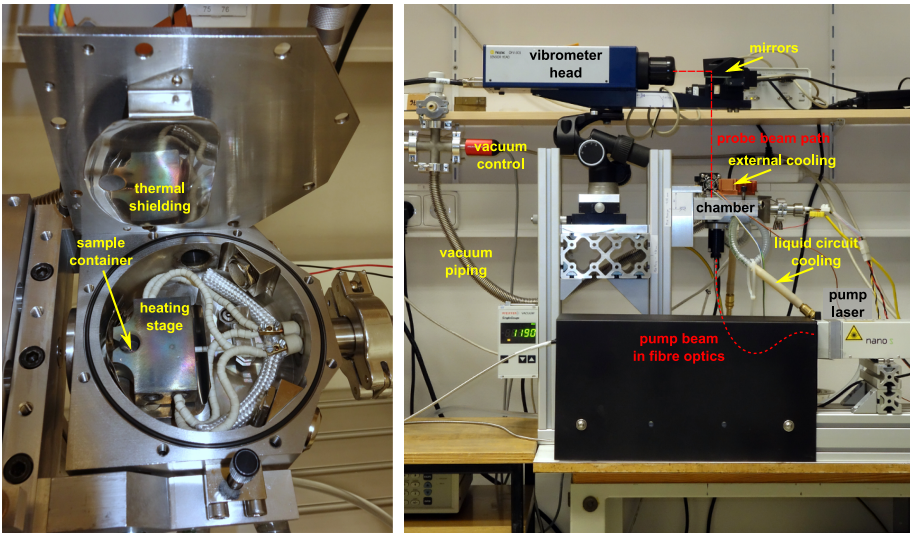

Figure 3: The vacuum chamber for high-temperature measurements (on the left) and the experimental setup for single-point RUS measurements using this chamber (on the right). The optical paths of the pump and probe lasers are outlined by dashed red lines. Photograph by J. Zídek.

ns, Litron, UK) an in-house-built temperature chamber with controlled atmosphere, and a Polytec OFV 505 laser vibrometer (Polytec, Germany). Similarly as for the previous arrangement, the pulse beam is driven to the chamber using fibre optics, and the probe laser beam records the vibrational response of the sample through a silica glass window in the upper wall of the chamber. This time, however, the vibrometer head is placed further away from the chamber (to avoid its possible exposure to excessive heat), and the positioning and focusing of the probe beam spot onto the upper face of the sample is done by an inclined mirror.

The chamber itself utilizes Joule heating for the temperature control, enabling the sample to reach temperatures up to $\sim$ 1000 K. Similarly as for the Peltier cascade, the heating module is computer driven, enabling stabilization and temperature control with a satisfying accuracy ($\pm$0.1 K). The cylindrical sample container is embedded in a bulk heating stage made of heat-resistant stainless steel. The heat transfer between the sample and the heating stage is

provided by a dilute nitrogen atmosphere. The outer walls of the chamber are cooled by a water circuit; in addition, a reflective shielding is placed above the heating stage to avoid direct radiation heat transfer from the stage to the upper wall of the chamber.

As mentioned above, this experimental arrangement can be used for measurements lasting for days or even weeks. Besides the above described simplifications, this brings some additional requirements. Most importantly, this arrangement must be equipped with an automated pressure control. At the beginning of the measurement, the dilute nitrogen atmosphere is set to a pressure of $\sim$ 10 mbar, which is enough for the heat transfer to the sample. During a long-term measurement, however, the pressure slowly increases due to evaporation of adsorbed gasses from the walls of the chamber a also some minor leakage. A computer-controlled valve is used ensure that the pressure never exceeds a chosen limit (typically set to 35 mbar). The setup also enables evacuating the chamber to $\sim 10^{-1}$ mbar and filling it with 10 mbar of dry nitrogen any time during the measurement, to avoid possible corrosion of the sample due to exposure of evaporated and leaked gasses. Furthermore, the whole device (temperature control, pressure control, vibrometer focusing, etc.) can be controlled remotely, using a VPN inteface, which is necessary for experiments running over several weeks.

The recorded data from the single-point high-temperature RUS arrangement are processed in a very similar manner as those from the modal RUS arrangement, using an in-house-built MATLAB toolbox. The software first loads the data from room-temperature measurements with scanned modal shapes (typically recorded before and after the high-temperature measurements), and then enables manual tracing of the chosen peaks with temperature and/or time. From the measured $\omega(T)$ dependences, the temperature evolutions of the elastic constants are then determined. Let us notice that the temperature shifts of the elastic constants can be determined with even higher accuracy than the constants themselves, as shown using the perturbation theory-based approach in [43].

The single-point high temperature RUS arrangement was used as the main experimental tool for papers [C1, C3, D2] included in the dissertation. Besides, it was used for e.g. monitoring of ageing processes in titanium alloys (not published yet), or for characterization of stability of microstructure and bonding quality of sprayed coatings [47, 48].

2.3 Line-source/point-receiver arrangement for measurements under uniaxial stress

The RUS method, in principle, enables measurements only in a stress-free state, as it follows from the boundary conditions requirement for (1). In several cases, however, also the evolution of elastic constants with pre-stress can be essential for understanding the mechanics of the examined material (e.g. [49, 50]). For such cases, the line-source/point-receiver arrangement described in this subsection has been developed.

The characterization of pre-stressed media using this arrangement is based on measuring the velocities of surface acoustic waves (SAWs) along a given direction at a given free surface of the sample. The velocites of SAWs in different directions are, again, dependent on the elastic constants and the mass density of the material. Hence for a set of SAW velocities $v_n^{\mathrm{exp}}(\mathbf{p}_n, \mathbf{q}_n)$, each corresponding to a propagation direction $\mathbf{q}_n$ and a free surface orientation $\mathbf{p}_n$ (i.e., $\mathbf{q}_n \perp \mathbf{p}_n$), one can write a similar objective function as (2), which is

$$F(C_{ijkl}) = \sum \left[v_n^{\mathrm{calc}}(\mathbf{p}_n, \mathbf{q}_n, C_{ijkl}, \rho) - v_n^{\mathrm{exp}}(\mathbf{p}_n, \mathbf{q}_n) \right]^2, \tag{4}$$

where the calculated velocity data v_n^{calc} are obtained, again, using a numerical simulation. As shown in [51], a suitable tool for this calculation can be the Ritz-Rayleigh method, which makes the inverse problem for SAWs (i.e., the minimization of (4)) very similar to the inverse problem for RUS. This similarity enables us to adopt most of the theoretical tools used for the RUS data analysis also for the SAW data analysis.

Let us point out that the velocities v_n^{calc} obtained by the Ritz-Rayleigh approach described in [51] are *phase velocity* data, while the data obtainable from LU measurements using a point-like source and point-like detector arrangement would be *group velocity* data in the directions given by the positions of the source and the detector. In anisotropic material, the phase velocity and group velocity may significantly differ, as the anisotropy leads to energy focusing along specific directions [52]. For this reason, the pump laser is focused into a line instead of into a point. The direction perpendicular to the line-like source and to $\mathbf{p}_n$ determines the wave vector direction of the propagating SAWs to $\mathbf{q}_n$, and the phase velocity can be determined by measuring times-of-flight of broadband pulse-like SAWs in a small number of points lying along the direction $\mathbf{q}_n$ [51]. By rotating the sample, SAW data for a set of $\mathbf{q}_n$-s can be achieved; if several differently oriented free surfaces are available for the measurement, several such sets can be obtained, each for one $\mathbf{p}_n$.

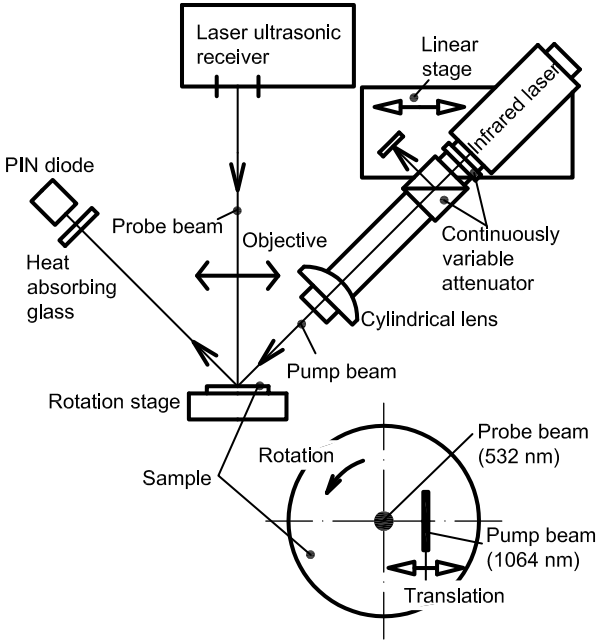

Figure 4: A schematic sketch of the line-source/point-receiver LU setup. Modified after [51].

The experimental arrangement for this technique is depicted in Fig.4. The particular instrumentation built and operated at IT-CAS is shown in Fig. 5. It consist of pulse laser (Nd:YAG, 1.064 μm, pulse energy 110 μJ, pulse duration 530 ps, STANDA, Lithuania), a rotation stage for the sample, and a broad-aperture laser vibrometer BossaNova TEMPO (1 GHz bandwidth, Bossa Nova Technologies, USA). The rotation stage can be further equipped with an in-house built testing machine allowing for unidirectional tensile/compressive loads up to 7 kN, mounted on the top of the stage, as seen in Fig.5. Hence, phase velocity maps $v_n^{\exp}(\mathbf{p}_n, \mathbf{q}_n)$ (typically for one or two $\mathbf{p}_n$-s determined by the faces of the sample) can be obtained for different stress levels.

The outputs of the measurement (i.e., sets of recorded signals at different stress levels) are further processed by a software developed at IT-CAS, enabling identification of SAW arrivals in each signal and, subsequently, inverse deter-

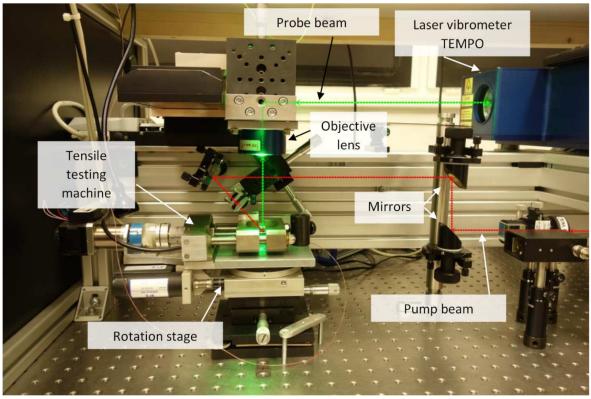

Figure 5: The experimental arrangement for line-source/point-receiver measurements under uniaxial stress. Modified after [53]. Photograph by J. Zídek.

mination of the elastic constants.

Notice that the methods based on SAWs are in principle less accurate than the RUS measurements, as they lack the resonant character of RUS. Hence, the line-source/point-receiver setup is suitable mainly in the cases when the changes of elasticity with pre-stress are pronounced (comparable with the values of the elastic constants themselves.) Furthermore, the device can currently operate only at the room temperature, which is controlled with accuracy ± 1 K by the air-conditioning system in the laboratory. Despite of these limitations, this experimental arrangement recently provided several unique data. Besides the results for the Fe-Pd shape memory alloy reported in the dissertation within the paper [A3], similarly interesting results were also observed for NiFeGaCo single crystals [53] and NiTi polycrystals [54]. Nowadays, the SAW-based LU methods are envisaged as the main direction for future development of the experiments at IT-CAS, with the ultimate aim to enable full characterization of anisotropic elasticity under temperature and stress. This may be of essential interest for understanding the behavior of crystalline materials close to their stability limits and critical points [55, 56].

3 Summary of results of the papers included in the dissertation

3.1 Ultrasonic characterization of shape memory alloys (papers [A1, A2, A3])

Shape memory alloys (SMAs,[57, 58, 59]) are an intriguing class of materials. These alloys exhibit several unique thermomechanical features, ranging from the shape memory effect itself to a gum-metal behavior [60]. All these features are results of the ability of these alloys to undergo thermoealstic martensitic transitions between the high-temperature phase called austenite, to the low temperature phase (or a variety of low-temperature phases) called martensite. SMAs belong among a broader class of solids called ferroelastics [61], exhibiting a transition between a paraelastic (entropy controlled) state and a ferroelastic state characterized by spontaneous strains breaking the symmetry of the paraelastic state. Within this class, however, the SMAs are those with the most apparent potential for applications, as they, in addition, exhibit several technologically favorable properties typical for metals, such as workability, electric conductivity, easy alloying, etc..

Mechanics of SMAs is a rich and still not fully explored research area, merging ideas from as distant disciplines as metallurgy and calculus of variation. The elastic constants of the individual phases play an important role here. Not only that the knowledge of elastic constants is required for designing applications of SMAs and simulating micromechanism of stress-strain behavior of SMAs. Even more importantly, the constants themselves are closely related to the martensitic transitions [62, 63], as these transitions are, using the terms from the theory of ferroelastics, *mediated by soft acoustic phonons*. In the terms of mechanics, this means that close to the transition temperatures or under mechanical loads close to thresholds for initiation of stress-induced transitions the crystal lattice of the given phase becomes extremely soft against shearing along some specific directions, which indicates the loss of stability of the lattice. This so-called shear softening or phonon softening is understood as a reliable precursor of the transition. Motivated by existence of these precursors, the elastic constants of SMAs have been extensively studied for decades now [64, 65, 66]. The softest shear constant of the austenite phase is typically the diagonal shear stiffness $c' = (c_{11} - c_{12})/2$.

The use of highly accurate and easily employable LU methods opens completely new possibilities in this direction. As mentioned in section 2, several LU

methods are particularly sensitive to shear elastic constants. Most apparently, the RUS method (see 2.1 and 2.2) is capable of very accurate determination of the softest shear elastic constant, i.e. the constant that exhibits phonon softening.

The papers [A1, A2, A3] included in the dissertation illustrate what various forms can the LU-based measurements of elastic constants of SMAs take. The first paper ([A1]) reports on determination of elastic moduli of thin SMA films undergoing a martensitic transition. This paper shows that the RUS method is capable of very accurate in-situ assessment of an elastic modulus of a supported film, enabling clear observation of the phonon softening of both the high-temperature phase and the low-temperature phase. In the second paper ([A2]), the ability of the RUS method to determine the full tensor of elastic constants is utilized. This paper shows that the stress-induced reorientation of a polycrystalline SMA (reorientaion is a mechanical process when the low-temperature phase becomes oriented such that it relaxes extrenal stresses) leads to a detectable and physically interpretable elastic anisotropy. Finally, the third paper ([A3]) shows the ability of SAW-based LU methods (see paragraph 2.3.) to characterize elastic anisotropy under stress. This measurement is done on a very specific SMA, exhibiting a so-called critical behavior [55, 56], enabling smooth (second order-like) transitions between the phases. Monitoring the evolution of elastic constants enables a unique deeper insight into the mechanism of the critical state, not achievable by any other method.

The main results can be summarized as follows: In [A1], we showed that the RUS method is capable of accurate determination of elastic constants of this surface films using an approach based on comparing the resonant spectra of a given substrate sample with and without the film (Figure 6(a-d)). By this approach, temperature evolutions of Young's moduli were obtained for three different films (Figure 6(e-g)). It was observed that these evolutions are both qualitatively and quantitatively very similar to the results obtained for bulk single crystals (see Figure 4 in [A1]) for a comparison.

The main result of [A2] can be best illustrated by Figure 7, showing the fundamental effect of elastic anisotropy of polycrystalline Ni-Ti alloy on the macroscopic stress-strain response of the material. Besides, the paper proves the RUS method to be able to detect small changes of anisotropy resulting from reorientation of martensite. Finally, the paper [A3] reports on a completely unique measurement, evaluating elastic anisotropy of a stress-induced tetragonalized state of the Fe-Pd alloy. Here, the main result is summarized in Figure 8, showing the evolution of soft acoustic phonon modes of with prestress in

a post-critical Fe-Pd alloy. It it seen that unlike for classical SMAs, where the these phonons typically soften with prestress (their slowness is increasing), here the softest phonons are stiffening (decreasing slowness), which confirms the post-ritical behavior. At the time the paper [A3] was published, it was not clear whether the soft phonon structure of the stress-induced tetragonalized lattice really corresponds to a soft phonon structure typical for tetragonal SMA martensites, as no measurements for such material were available in the literature. Some confirmation of this hypothesis was brought two years later by Sedlák et al.[68] (applicant being the corresponding author), who reported on elastic constants of non-modulated tetragonal NiMnGa martensite. Indeed, this materials exhibited exactly the same orientation of soft shearing modes as the teragonalized state of the Fe-Pd alloy.

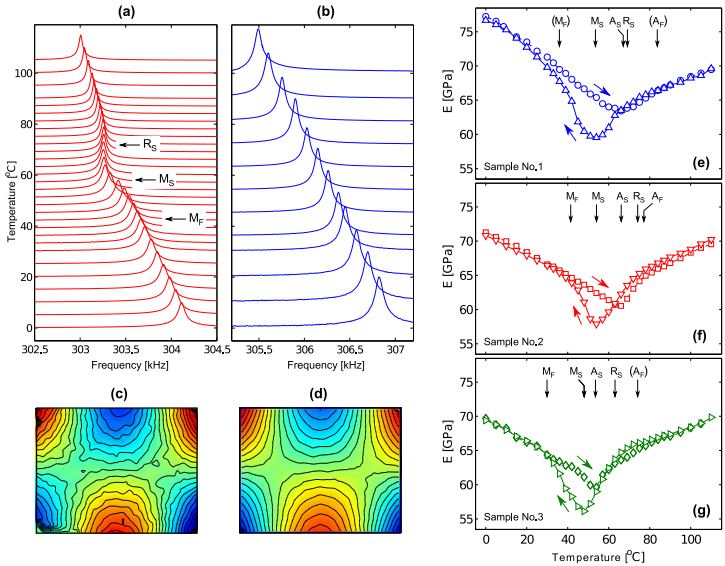

Figure 6: A summary of results of paper [A1]: (a,b) temperature evolutions of a chosen RUS resonant peak with and without the film; (c,d) the corresponding modal shapes; (e,f,g) resulting evolutions of Young's modulus for three different films. The labels $(\mathrm{A}, \mathrm{R}, \mathrm{M})_{(\mathrm{S},\mathrm{F})}$ refer to start and finish temperatures for austenite, R-phase and martensite, respectively.

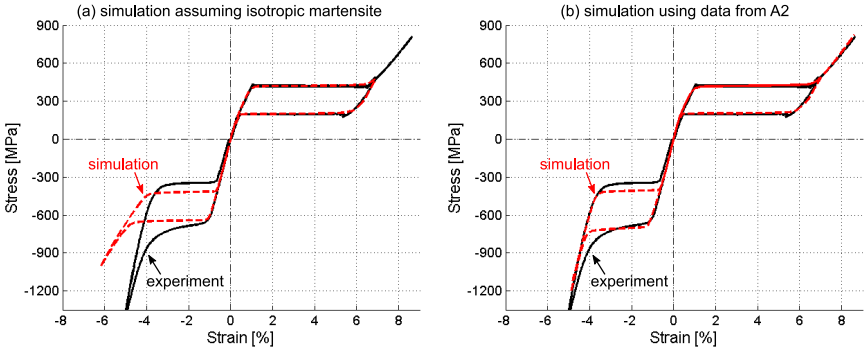

Figure 7: A comparison of the simulation and experiment for unidirectional tension/compression tests of polycrystalline NiTi using the constitutive model described in [67]: (a) simulation assuming isotropic elastic constants for polycrystalline martensite; (b) simulation assuming anisotropic elasticity of martensite developing with reorientation, as described in [A2]. Graphs courtesy of P. Sedlák.

3.2 Ultrasonic characterization of materials with strong magnetoelastic coupling - the case of FSMA high-temperature phases (papers [B1, B2, B3])

Similarly to the ferroelastic phase transitions, the *magnetostriction*, i.e. the spontaneous straining of the crystal unit cell due to rotation of the magnetization vector, may have a significant impact on the elastic constants. For materials with strong magnetostriction but weak magnetocrystalline anisotropy, the so-called δE effect emerges [69]. This effect can be observed as an anomalous decrease of Young's modulus of the material for strain amplitudes below the magnitude of magnetostriction. The physical reason for this phenomenon is obvious: For such small amplitudes, the part of the externally imposed strains can be relaxed by rotation of the magnetization vector. Such a coupling between strain and magnetization is called the *magnetoelastic coupling*.

Apparent examples of materials exhibiting high magnetostriction and weak magnetocrystalline anisotropy are the high-temperature phases (austenites) of ferromagnetic shape memory alloys (FSMAs), namely FSMAs with Heusler-type atomic ordering [70]. The reason is that in Heusler alloys the magnetization vector field can be strongly destabilized by crystal defects, in particular the anti-phase boundaries (APBs, see [71, 72] for examples and physical reason-

ing), which leads to a significant decrease of magnetocrystalline anisotropy. At the same time, the austenites of FSMAs have soft shearing modes due to their ability to undergo the thermoelastic martensitic transitions upon cooling; this means that their unit cells can get easily deformed along the cubic-to-tetragonal path. This amplifies the effect of the magnenization vector on the lattice parameters and results in relatively high magnetostriction [73].

The LU methods can be utilized to analyze the lattice softening due to magnetoelastic coupling using very similar approaches as for phonon softening in conventional SMAs. As discussed by Heczko et al. [74] (applicant being among

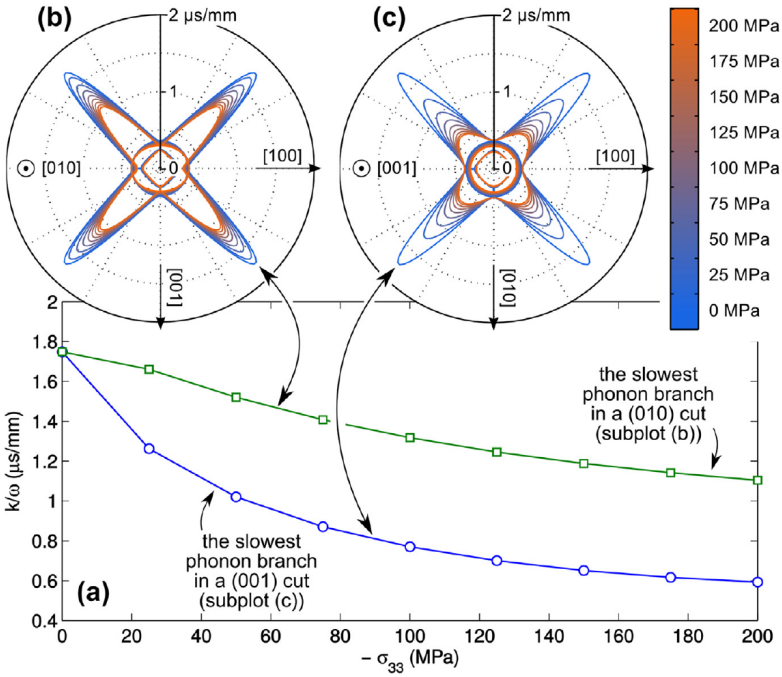

Figure 8: Evolutions of soft acoustic phonons (slowest transversal acoustic modes) for the Fe-Pd single crystal studied in [A3]. As seen in (a), both phonons exhibit decrease in slowness, which means stiffening. Polar plots of the slowness curves in two principal cuts are seen in (b) and (c). Modified after [A3].

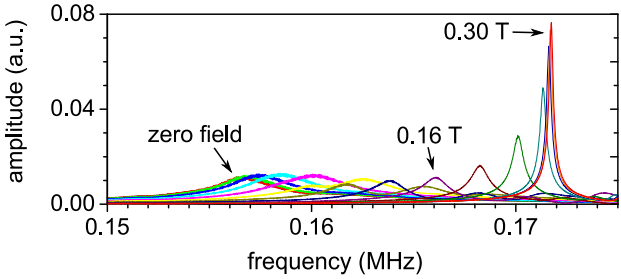

Figure 9: Evolution of a chosen resonant peak in RUS measurement with increasing external field (modified after [74]). The field suppresses the rotations of the magnetization vector, which leads to stiffening (i.e., increase of the resonant frequency) and decrease of magnetoelastic damping (i.e. decrease of the peak width). The shown example was measured on Ni-Mn-Ga premartesite at 240 K.

the co-authors), especially the RUS method is a suitable tool for analyzing the magnetoelastic phenomena (see Figure 9). Three papers showing examples of such analyses are included in the dissertation, the first two [B1, B2] being done on the most prototypical FSMA, which is Ni-Mn-Ga, and the last one [B3] on a more unusual alloy Co-Ni-Al. The first two are fully focused on the RUS measurements for the given alloy, the third one brings also several detail on microstructure, heat treatment, transition temperatures, and other properties of the Co-Ni-Al alloy.

In two respects, the characterization of magnetoelastic coupling in FSMAs by means of RUS is more intricate than just the characterization of phonon softening in conventional SMAs. The first difference is that the magnetoelastic coupling is manifested not only by elastic softening, but also by a significant increase of damping. On one hand, this helps us to detect the coupling; on the other hand, extensive damping may lead to much more difficult RUS spectra analysis, due to overlapping of the peaks and lower signal-to-noise ratio. The second difference is that, in order to obtain more complete information, some of the RUS measurements must be done in an external magnetic field. This brings some additional technical difficulties - the sample must be prevented from rotating along the field (and thus, the ideal stress-free boundary conditions for the vibrations are necessarily broken), and also the temperature control cannot be provided by the vacuum chambers described in section 2, as

they do not allow the sample to be placed in a sufficiently homogeneous magnetic field. The papers in this section bring, thus, a mixture of results obtained in zero field using the RUS arrangement described in paragraph 2.1, and those obtained using more dedicated RUS arrangements for measurements in the field.

The main results of papers [B1] and [B2] are seen in Figure 10. The soft elastic coefficient c' exhibits different softening trends depending on the external field and on the heat treatment (illustrating the role of defects in the quenched material). It is seen that the softening can be clearly decomposed into the phonon-induced one (being nearly the same for both materials) that appears in saturated magnetic field, and the one resulting from magnetoelastic coupling.

Figure 11 shows the same effect for the CoNiAl alloy [B3], where the magnetic transition (i.e., the Curie point) is spread over a broader temperature range due to complex microstructures appearing in this alloy. Again, the paper [B3] proves that RUS can be used as a tool for decomposing phonon-mediated

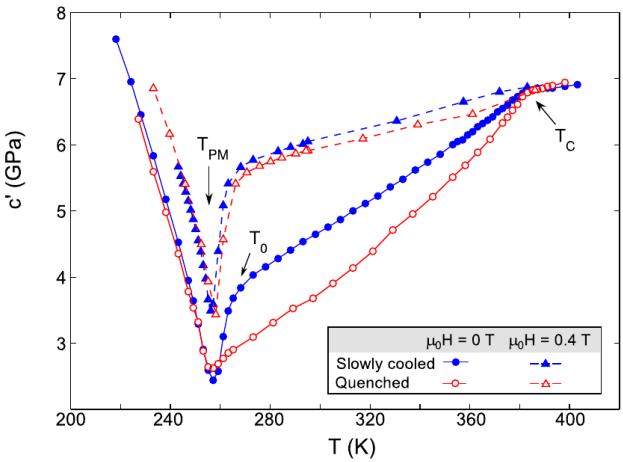

Figure 10: Summary of results of papers [B1] and [B2]: $c'(T)$ softening curves upon cooling with and without external magnetic field. Results for two materials are shown; the quenched material has higher desity of defects, which increases the magnetoelastic coupling effects. $\mathrm{T_C}$ and $\mathrm{T_{PM}}$ denote the Curie point and the premartensitic transition temperature, respectively.

and magnetoelastic softening, utilizing its genuine sensitivity to the softest shear coefficient c'

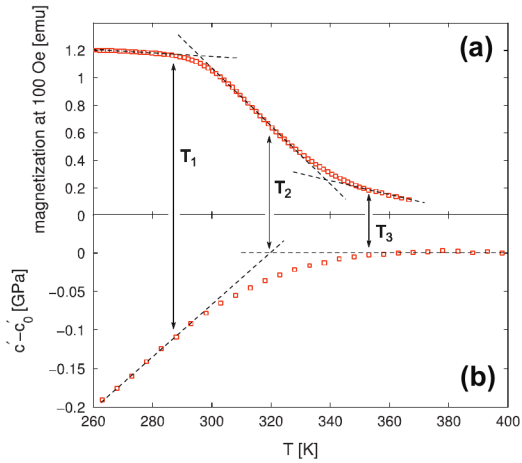

Figure 11: Temperature evolutions of the magnetization (a) and soft shear elastic modulus c' for the CoNiAl ferromagnetic shape memory alloy. In (b), c'_0 stands for the c' coefficient unaffected by magnetoelastic softening, i.e. having the $\mathrm{d}c'/\mathrm{d}T$ slope given solely by phonon-mediated softening.

3.3 Ultrasonic characterization of materials with diffusive phase transitions - the case of embedded particles

Unlike the martensitic transitions, the diffusive transitions are not preceded by any softening of acoustic phonons, and so there is no obvious reason for using them for monitoring the transformation process instead of more conventional methods, such as differential scanning calorimetry (DSC) or resistivity measurements, or instead of diffraction-based methods that directly provide also some information on the crystal structure.

The only case where the ultrasonic methods are irreplaceable is when the diffusive transition appears just in very small volumes inside of the material (cf. [75, 76, 77]), i.e. in small particles embedded in the crystal lattice. Then, the RUS method, which is sensitive to even very small changes of the properties

of the material, can give much more reliable information on the onset of the transition as well as on its evolution in time.

The dissertation includes three papers illustrating such an approach. In [C1], the analyzed material is a free-cutting aluminum alloy with small meltable particles inside the material. These particles melt at much lower temperatures than the melting temperature of the matrix. Due to the very small volume fraction of the particles ($< 1\%$), the DSC characterization becomes unreliable. We show, however, that the RUS method can detect the melting and solidification of the particles very accurately, and, based on the RUS results, we can discuss the origin of the melting-solidification asymmetry and the evolution of the transition temperatures with cycling.

The other two papers, [C2] and [C3], are concerned with a slightly different topic. In metastable $\beta-$titanium alloys [78, 79], annealing at moderate temperatures leads to nucleation and growth of nanometric particles of the isothermal ω phase. Neither the volume fraction, nor the kinetics of the growth can be reliably detected by any diffraction measurements, since the ω phase is fully coherent with the $\beta-$matrix, and thus, most of the diffraction peaks of these phases coincide. Some information can be obtained from the electrical resistivity; however, as we show in [C2] and [C3], the most reliable quantita-

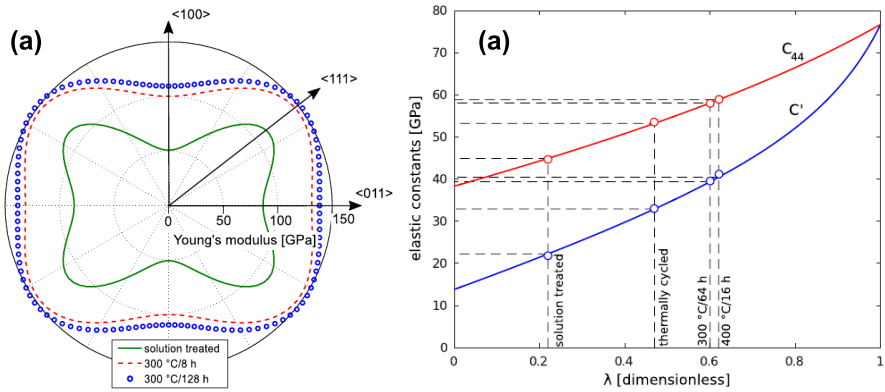

Figure 12: Main results of papers [C2] and [C3]: (a) the effects of $\omega-$particles growth on anisotropy and magnitude of Young's modulus of Timetal LCB single crystals; (b) the same effect on shear elastic moduli of Ti-15Mo single crystals. In both cases, the growth leads to strong stiffening and isotropization.

tive information can be assessed from laser-based RUS measurements (Figure 12). More precisely, as discussed in [80], the RUS measurements are complementary to the resistivity measurements, as the resistivity is more sensitive to the presence of phase interfaces, and the RUS measurement to the volume fraction of the individual phases.

3.4 Ultrasonic characterization of materials processed by severe plastic deformation

The last section of the dissertation discusses the applications of LU methods for polycrystalline materials with high volume fraction of grain boundaries (GBs). For a polycrystal with the grain size of several μm or larger, the GBs can be considered as of zero volume, having only a negligible effect on the macro-scale elastic constants or macro-scale internal friction parameters. When the grains are nanoscopic, however, the boundaries may start playing a dominant role. The well-established homogenization theory for polycrystals [83, 84] typically assumes that the macro-scale elastic constants of a polycrystalline aggregate can be calculated from the orientation distribution function (ODF) and from a statistical description of the shapes of the grains, possibly involving also correlations between these two parameters [85]. This theory, however, obviously cannot capture the case of ultrafine-grained materials, such as those processed by severe plastic deformation (SPD,[86, 87]), where the properties may be strongly affected by GBs. The relation between the microstructure and the macro-scale elastic properties then becomes unclear and calls for an experimental investigation.

The papers [D1, D2, D3] represent three examples of laser-based RUS characterization of such materials, revealing, in some respect, a surprising role of GBs. In the first case ([D1], polycrystalline copper processed by Equal Channel Angular Pressing, ECAP [88, 89]) we showed that the elastic constants of such a material can adopt a symmetry class resulting neither from the processing directions, nor from the crystallographic texture, but from the dominant orientation of GBs and the shape of the grains. For this analysis, we utilized the ability of LU methods to determine the elastic constants of a generally anisotropic (triclinic) solid, verified later on benchmark examples in [37]. This means that the result in [D1] might not be possible to obtain by any other experimental method. The most illustrative result from [D1], i.e. the result for a material after one ECAP pass (denotes 1P1 in [D1]) is given in Figure 13, showing the estimated material symmetry from the elastic constants and the corresponding

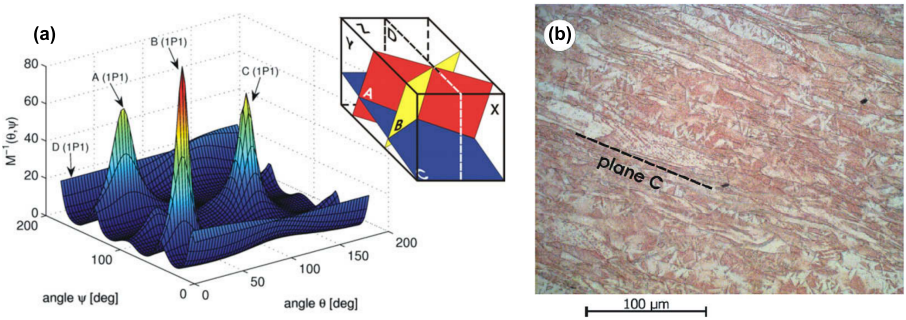

Figure 13: Symmetry class determination based on elastic constants for fine-grained polycrystalline copper: (a) a function measuring the level of mirror symmetry of elastic properties over a plane with a normal vector given by Euler angles ψ and θ; (b) optical microscopy of the microstructure showing significant grain elongation along the plane identified in (a). Modified after [D1].

microstructure.

In the second paper ([D2], the AZ31 magnesium alloy processed by ECAP), we showed that the LU methods can provide very valuable information on the GBs themselves, in particular on grain boundary sliding, which is a dominant mechanism of superplastic forming of the examined alloy [90, 91]. Based on the RUS data, we were able to determine the activation energy and the onset temperature for a dominant GB mechanism, and correlate these parameters with grain size. The resulting data revealed a nearly linear dependence between these two parameters over a broad range of grain sizes (Figure 14).

The third paper included in the dissertation, [D3], shows that the LU methods can be also utilized for a completely opposite task: to prove that the grain boundaries may not affect the elastic anisotropy at all. The studied materials are cold-sprayed metallic deposits [92, 93] with a very dominant GB orientation, resultant from the spraying process. The impact-induced severe plastic deformation inside of the individual grains [94], however, adds enough randomness to the microstructure such that resulting polycrystalline aggregate is perfectly isotropic. From the materials science point of view, this paper brought data confirming that cold-spraying can produce materials with elastic properties very close to bulk polycrystals.

The potential use of the LU methods and ultrasonic methods in general for finely grained materials is, however, much broader that what illustrated by the

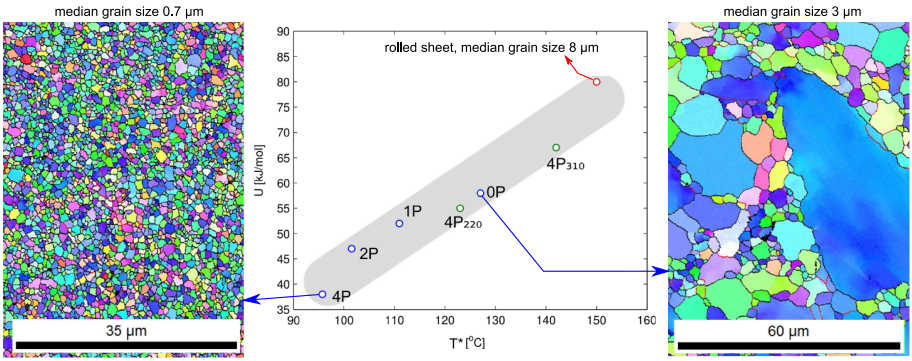

Figure 14: Correlation between activation energy U and onset temperature $T*$ for GB sliding in the AZ31 alloy revealed by ultrasonic measurements. Individual points in the graph represent samples with different levels of grain refinement, for the smallest (4P) and largest (0P) grains, EBSD maps of the microstructure are given. Modified after [D2].

chosen three papers. As observed already by Kobelev et al. [95], the grain refinement leads to a weak but detectable decrease of the elastic modulus, probably due to an increased amount of amorphous phase coming from the GBs. This fact was utilized by the applicant's research team for example for characterization of heterogeneous grain refinement in materials processed by high-pressure torsion [96], or for in-situ monitoring of recrystallization in cold-sprayed materials [48]. Another example can be found in [97], where the applicant and his team used the RUS measurements for an in-situ detection of surface micro-cracking in ECAPed AZ31 when subjected to temperatures below the freezing point. Again, as the micro-cracking affects only a very small volume fraction of the material, detecting this process in-situ by any other experimental method might not be reliable or even possible, while in RUS a two-orders-of-magnitude increase in the internal friction parameter is observed (Figure 15).

Finally, let us notice that the paper [D3], in some sense, also well illustrates the limitations of the RUS method and of the LU approaches themselves. Despite the perfect elastic isotropy, the cold-sprayed coatings systematically exhibit anisotropic fracture toughness [98]. Similarly, the extruded/ECAPed magnesium alloys [D2, 99] can have strongly anisotropic yield stress while ex-

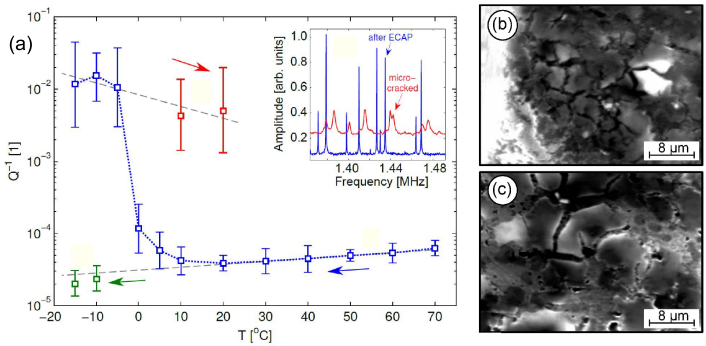

Figure 15: Detection of surface micro-cracking of finely grained AZ31: (a) an evolution of RUS spectra along a temperature cycle; (b,c) micro-cracked regions along the edges of the sample. The green experimental points in the lower left corner of (a) were obtained for a sample with a special surface treatment that prevented micro-cracking. Modified after [97].

hibiting a perfect elastic isotropy. In other words, while the elastic constants obtained by the LU methods may be very good indicators of some processes in the examined materials, it must be always taken into account that they characterize the behavior of the material at very low strain amplitudes and in a fast (adiabatic) regime. The LU methods, in spite of their versatility and power, can thus, never replace classical destructive methods of experimental mechanics.

4 Concluding remarks and future outlook

The above given and commented set of papers can be understood as a proof of how broad is the range of materials science topics the LU measurements can cover, and what new insights can the LU methods bring. At the same time, it can be understood as a motivation for further development of these methods and for exploring new possible areas for their applications.

Under the applicant's leadership, the Department of Ultrasonic Methods ITCAS currently aims for utilizing the LU approaches in several new directions. Among them, the most intriguing are:

1. **going beyond the homogeneity assumption** – the applicant is currently a PI of the Czech Science Foundation project entitled *Advanced laser-*

ultrasonic characterization of structural transitions in metals – analysis beyond the homogeneity assumption, where the main aim is to explore the ability of LU methods to characterize materials heterogeneous at the lengthscales comparable to the wavelength. This covers e.g. a characterization of embedded planar interfaces in multi-layered composites (in collaboration with ICV-CSIC Madrid, Spain), laminate-type microstructures in shape memory alloys (in collaboration with Tohoku University, Japan), or functionally graded titanium alloys (in collaboration with Charles University). Several types of heterogeneity are considered (Figure 16), especially those that may appear during phase transitions on metallic materials, or, vice-versa, artificially created heterogeneities that can significantly affect the phase transition mechanism.

2. **going beyond the linearity assumption** – the non-linear ultrasonic characterization is a self-sustained field of non-destructive testing of materials [100, 101], where also the LU-based approaches can be utilized. However, the direction the applicant's team is currently planning to follow is much more oriented on the fundamental research: studying material with inherently non-linear stress-strain response, resulting for example from the precursor softening or from the presence of highly mobile ferroelastic domain walls in SMAs. Preliminary results (Figure 17) indicate that both the laser-based RUS measurements or the TGS measurements may be able to detect and quantify such non-linearity. This opens a completely new possibilities and posts new challenges for LU-based charac-

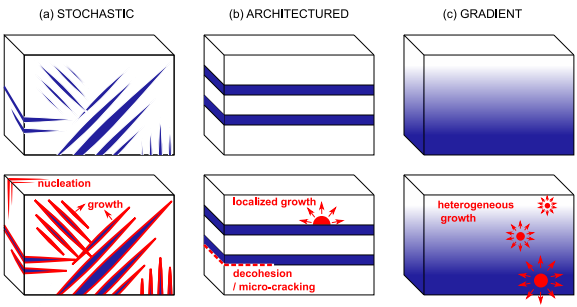

Figure 16: Types of heterogeneities (upper row) and the thermally activated processes in them (lower row) to be studied in the current research project lead by the applicant.

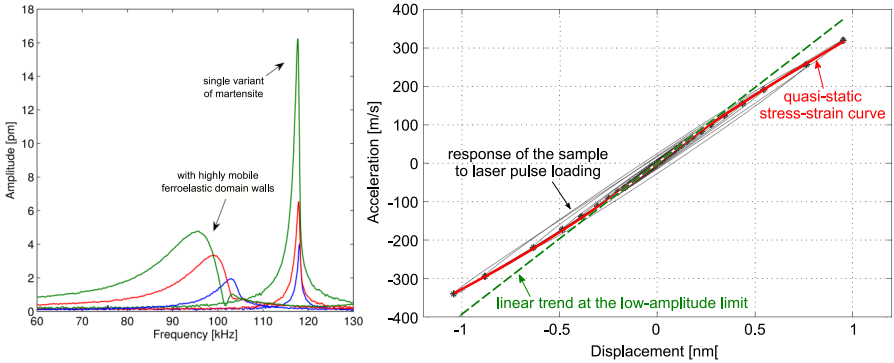

Figure 17: Nonlinear stress-strain character of a Ni-Mn-Ga FSMA single crystal in the martensite phase. On the left: difference in RUS spectra with and without the highly mobile ferroelastic domain walls, different colors refer to different pump beam amplitudes. On the right: the stress-strain curve estimated from the RUS measurements. Modified after [102].

terization, requiring a quantitative assessment of strain amplitudes and advanced signal processing.

These new directions may even broaden the range of applicability of the currently utilized LU methods, but they also might (and nearly certainly they will) also initiate completely new LU-based concepts. This is the research philosophy the applicant wanted to be illustrated by this dissertation. The LU methods, in principle, are always rather demanding regarding both their instrumentation and the processing and interpretation of the recorded experimental data. For these reasons, most of the LU-based approaches will never become broadly used or commercially available. But they are consistently getting the recognition they deserve from the point of view of fundamental research in the field of experimental mechanics and characterization of materials; all papers included in this dissertation somehow aimed to contribute to this recognition.

Bibliography

Papers included in the dissertation:

[A1] Thomasová, M., Sedlák, P., Seiner, H., et al. (2015) Scripta Materialia, 101, pp. 24-27.

[A2] Thomasová, M., Seiner, H., Sedlák, P., et al. (2017) Acta Materialia, 123, pp. 146-156.

[A3] Seiner, H., Stoklasová, P., Sedlák, P., et al. (2016) Acta Materialia, 105, pp. 182-188.

[B1] Seiner, H., Heczko, O., Sedlák, P., et al. (2013) Journal of Alloys and Compounds, 577 (SUPPL. 1), pp. S131-S135.

[B2] Seiner, H., Sedlák, P., Bodnárová, L., et al. (2013) Journal of Physics Condensed Matter, 25 (42), art. no. 425402.

[B3] Seiner, H., Kopeček, J., Sedlák, P., et al. (2013) Acta Materialia, 61 (15), pp. 5869-5876. (IF=7.293, 16 citations. The applicant was the first author.)

[C1] Nejezchlebová, J., Seiner, H., Ševčík, M., et al. (2015) NDT and E International, 69, pp. 40-47.

[C2] Nejezchlebová, J., Janovská, M., Seiner, H., et al. (2016) Acta Materialia, 110, pp. 185-191.

[C3] Nejezchlebová, J., Janovská, M., (...), Seiner, H. (2019) Journal of Alloys and Compounds, 792, pp. 960-967.

[D1] Seiner, H., Bodnárová, L., Sedlák, et al. (2010) Acta Materialia, 58 (1), pp. 235-247.

[D2] Koller, M., Sedlák, P., Seiner, H., et al. (2014) Journal of Materials Science, 50 (2), pp. 808-818.

[D3] Seiner, H., Cizek, J., Sedlák, P., et al. (2016) Surface and Coatings Technology, 291, pp. 342-347.

References:

[1] Christoffel, E.B. (1877) Annali di Matematica Pura ed Applicata, 8 (1), pp. 193-243.

[2] Musgrave, M.J.P., Crystal Acoustics. 1st edition, San Francisco: Holden-Day, 1970.

[3] Auld, B.A., Acoustic fields and waves solids, Vol.1. 1st edition, New York: John Wiley and Sons, 1973.

[4] Every, A.G., Sachse, W. (Eds.), Dynamic methods for measuring the elastic properties of solids, (Handbook of elastic properties of solids, liquids and gases, Volume I.) San Diego: Academic Press, 2001.

[5] François, M., Geymonat, G., Berthaud, Y. (1998) International Journal of Solids and Structures, 35 (31-32), pp. 4091-4106.

[6] Scruby, C.B. (1989) Ultrasonics, 27 (4), pp. 195-209.

[7] Dewhurst, R.J., Shan, Q. (1999) Measurement Science and Technology, 10 (11), pp. R139-R168.

[8] Achenbach, J.D. (2000) International Journal of Solids and Structures, 37 (1-2), pp. 13-27.

[9] Aussel, J.-D., Monchalin, J.-P. (1989) Ultrasonics, 27 (3), pp. 165-177.

[10] Zadler, B.J., Le Rousseau, J.H.L., Scales, J.A., et al. (2004) Geophysical Journal International, 156 (1), pp. 154-169.

[11] Nadal, M.-H., Hubert, C., Oltra, R. (2009) Journal of Applied Physics, 106 (2), art. no. 024906.

[12] Matsumoto, T., Nose, T., Nagata, Y., et al. (2001) Journal of the American Ceramic Society, 84 (7), pp. 1521-1525.

[13] Chigarev, N., Zinin, P., Ming, L.-C., et al. (2008) Applied Physics Letters, 93 (18), art. no. 181905.

[14] Nikitin, S.M., Tournat, V., Chigarev, N., et al. (2014) Journal of Applied Physics, 115 (4), art. no. 044902.

[15] Wright, O.B., Matsuda, O., Perrin, B., et al. (2001) Physical Review B - Condensed Matter and Materials Physics, 64 (8), art. no. 081202.

[16] Matsuda, O., Wright, O.B., Hurley, D.H., et al. (2004) Physical Review Letters, 93 (9), pp. 095501-1-095501-4.

[17] Pierce, R., Ume, C., Jarzynski, J. (1995) Ultrasonics, 33 (2), pp. 133-137.

[18] Grünsteidl, C., Veres, I.A., Roither, J., et al. (2013) Applied Physics Letters, 102 (1), art. no. 011103.

[19] Carome, E.F., Clark, N.A., Moeller, C.E. (1964) Applied Physics Letters, 4 (6), pp. 95-97.

[20] Ready, J.F. (1965) Journal of Applied Physics, 36 (2), pp. 462-468.

[21] Gournay, L.S. (1966) Journal of the Acoustical Society of America, 40 (6), pp. 1322-1330.

[22] White, R.M. (1963) Journal of Applied Physics, 34 (12), pp. 3559-3567.

[23] Li, C., Guan, G., Zhang, F., et al. (2014) Biomedical Optics Express, 5 (12), pp. 4313-4328.

[24] Li, C., Guan, G., Zhang, F., et al. (2014) Biomedical Optics Express, 5 (5), pp. 1403-1418.

[25] Bauer-Marschallinger, J., Berer, T., Grun, H., et al. (2012) IEEE Transactions on Ultrasonics, Ferroelectrics, and Frequency Control, 59 (12), art. no. 6373786, pp. 2631-2645.

[26] Remillieux, M.C., Ulrich, T.J., Payan, C., et al. (2015) Journal of Geophysical Research: Solid Earth, 120 (7), pp. 4898-4916.

[27] Shragge, J., Blum, T.E., van Wijk, K., et al. (2015) Geophysics, 80 (6), pp. D553-D563.

[28] Mi, B., Ume, C. (2006) Journal of Manufacturing Science and Engineering, Transactions of the ASME, 128 (1), pp. 280-286.

[29] Jen, C.-K., Moisan, J.-F., Zheng, C.-Q., et al. (2004) Ultrasonics, 41 (10), pp. 777-784.

[30] Bienville, T., Robillard, J.F., Belliard, L., et al. (2006) Ultrasonics, 44 (SUPPL.), pp. e1289-e1294.

[31] Jean, C., Belliard, L., Becerra, L., et al. (2015) Applied Physics Letters, 107 (19), art. no. 193103.

[32] Guilbaud, S., Audoin, B. (1999) Journal of the Acoustical Society of America, 105 (4), pp. 2226-2235.

[33] Monchalin, J.-P., Aussel, J.-D. (1990) Journal of Nondestructive Evaluation, 9 (4), pp. 211-221.

[34] Hofmann, F., Short, M.P., Dennett, C.A. (2019) MRS Bulletin, 44 (5), pp. 392-402.

[35] Duncan, R.A., Hofmann, F., Vega-Flick, A., et al. (2016) Applied Physics Letters, 109 (15), art. no. 151906.

[36] Grabec, T., Sedlák, P., Stoklasová, P., et al. (2016) Smart Materials and Structures, 25 (12), art. no. 127002.

[37] Sedlák, P., Seiner, H., Zídek, J., et al. (2014) Experimental Mechanics, 54 (6), pp. 1073-1085.

[38] Nowick, A.S., Berry B.S. Anelastic relaxation in crystalline solids. New York: Academic Press, 1972.

[39] Migliori, A., Sarrao, J.L., Visscher, W.M., et al. (1993) Physica B: Physics of Condensed Matter, 183 (1-2), pp. 1-24.

[40] Leisure, R.G., Willis, F.A. (1997) Journal of Physics Condensed Matter, 9 (28), pp. 6001-6029.

[41] Seiner, H., Sedlák, P., Koller, M., et al. (2013) Composites Science and Technology, 75, pp. 93-97.

[42] Ogi, H., Sato, K., Asada, T., et al. (2002) Journal of the Acoustical Society of America, 112 (6), pp. 2553-2557.

[43] Landa, M., Sedlák, P., Seiner, H., et al. (2009) Applied Physics A: Materials Science and Processing, 96 (3), pp. 557-567.

[44] Janovská, M., Sedlák, P., Kruisová, A., et al. (2015) Journal of Physics D: Applied Physics, 48 (24), art. no. 245102.

[45] Kruisová, A., Seiner, H., Sedlák, P., et al. (2014) Applied Physics Letters, 105 (21), art. no. 211904.

[46] Boyer, H.E., Gall, T.L., Metals Handbook, Metals Park, OH: American Society for Metals, 1985.

[47] Janovská, M., Sedlák, P., Cizek, J., Koller, M., Šiška, F., Seiner, H. et al. (2020) Ultrasonics, 106, art. no. 106140.

[48] Janovská, M., Seiner, H., Čížek, J., et al. (2018) Acta Physica Polonica A, 134 (3), pp. 794-798.

[49] Kato, M., Sato, T., Ando, K. (1997) Journal of the Acoustical Society of America, 101 (4), pp. 2111-2121.

[50] Thurston, R.N., Brugger, K. (1964) Physical Review, 133 (6A), pp. A1604-A1610.

[51] Stoklasová, P., Sedlák, P., Seiner, H., et al. (2015) Ultrasonics, 56, pp. 381-389.

[52] Wolfe, J.P., Imaging Phonons. Cambridge: Cambridge University Press, 1998.

[53] Zoubková, K. Elastic response of ferromagnetic shape memory alloys in the vicinity of the critical point. Diploma thesis, Czech Technical University in Prague, 2019.

[54] Grabec, T., Zoubková, K., Stoklasová, P.,et al. (2018) Acta Physica Polonica A, 134 (3), pp. 811-814.

[55] Kosogor, A., L'vov, V.A., Chernenko, V.A.,et al. (2014) Acta Materialia, 66, pp. 79-85.

[56] Chernenko, V.A., L'vov, V.A., Kabra, S., et al. (2018) Physica Status Solidi (B) Basic Research, 255 (2), art. no. 1700273.

[57] Otsuka, K., Wayman, C.M. (Eds.)Shape memory materials. Cambridge: Cambridge University Press, 1998.

[58] Bhattacharya, K. Microstructure of Martensite. Oxford: Oxford University Press, 2003.

[59] Mohd Jani, J., Leary, M., Subic, A., et al. (2014) Materials and Design, 56, pp. 1078-1113.

[60] Ren, X., Otsuka, K. (1997) Nature, 389 (6651), pp. 579-582.

[61] Salje, E.K.H., Hayward, S.A., Lee, W.T. (2005) Acta Crystallographica A, 61 (1), pp. 3-18.

[62] Nakanishi, N. (1980) Progress in Materials Science, 24 (C), pp. 143-265.

[63] Lüthi, B. Physical Acoustics in the Solid State, Berlin/Heidelberg: Springer-Verlag, 2005.

[64] Brill, T.M., Mittelbach, S., Assmus, W., et al. (1991) Journal of Physics: Condensed Matter, 3 (48), art. no. 004, pp. 9621-9627.

[65] Sedlák, P., Seiner, H., Landa, M., et al. (2005) Acta Materialia, 53 (13), pp. 3643-3661.

[66] González-Comas, A., Mañosa, L., Planes, A., et al. (1997) Physical Review B, 56 (9), pp. 5200-5206.

[67] Sedlák, P., Frost, M., Benešová, B., et al. (2012) International Journal of Plasticity, 39, pp. 132-151.

[68] Sedlák, P., Seiner, H., Bodnárová, L., et al. (2017) Scripta Materialia, 136, pp. 20-23.

[69] Chikazumi, S., Graham, C. Physics of Magnetism. Huntington, NY: Krieger, 1978.

[70] Webster, P.J. Heusler alloys (1969) Contemporary Physics, 10 (6), pp. 559-577.

[71] Lapworth, A.J., Jakubovics, J.P. (1974) Philosophical Magazine, 29 (2), pp. 253-273.

[72] Young, A.P., Jakubovics, J.P. (1975) Journal of Physics F: Metal Physics, 5 (10), art. no. 010, pp. 1866-1883.

[73] Tickle, R., James, R.D. (1999) Journal of Magnetism and Magnetic Materials, 195 (3), pp. 627-638.

[74] Heczko, O., Seiner, H., Sedlák, P., et al. (2013) European Physical Journal B, 86 (2), art. no. 62.

[75] Borisov, B.F., Charnaya, E.V., Hoffmann, W.D., et al. (1997) Journal of Physics Condensed Matter, 9 (16), pp. 3377-3386.

[76] Charnaya, E.V., Plotnikov, P.G., Michel, D., et al. (2001) Physica B: Condensed Matter, 299 (1-2), pp. 56-63.

[77] Borisov, B., Charnaya, E., Plotnikov, P., et al. (1998) Physical Review B, 58 (9), pp. 5329-5335.

[78] Lütjering, G., Williams, J.C. Titanium, 2nd edition, Berlin/New York:Springer, 2007.

[79] Grosdidier, T., Philippe, M.J. (2000) Materials Science and Engineering A, 291 (1), pp. 218-223.

[80] Nejezchlebová, J., Seiner, H., Sedlák, P., et al. (2018) Journal of Alloys and Compounds, 762, pp. 868-872.

[81] Demarest, H.H. (1971) Journal of the Acoustical Society of America, 49 (3B), pp. 768-775.

[82] Šmilauerová, J., Harcuba, P., Stráský, J., et al. (2014) Acta Materialia, 81, pp. 71-82.

[83] Hashin, Z., Shtrikman, S. (1963) Journal of the Mechanics and Physics of Solids, 11 (2), pp. 127-140.

[84] Hashin, Z. (1960) Journal of Applied Mechanics, Transactions ASME, 29 (1), pp. 143-150.

[85] Saheli, G., Garmestani, H., Gokhale, A. (2008) Journal of Mechanics of Materials and Structures, 3 (1), pp. 85-106.

[86] Valiev, R.Z., Islamgaliev, R.K., Alexandrov, I.V. (2000) Progress in Materials Science, 45 (2), pp. 103-189.

[87] Valiev, R. (2004) Nature Materials, 3 (8), pp. 511-516.

[88] Valiev, R.Z., Langdon, T.G. (2006) Progress in Materials Science, 51 (7), pp. 881-981.

[89] Iwahashi, Y., Wang, J., Horita, Z., et al. (1996) Scripta Materialia, 35 (2), pp. 143-146.

[90] Abu-Farha, F.K., Khraisheh, M.K. (2007) Advanced Engineering Materials, 9 (9), pp. 777-783.

[91] Panicker, R., Chokshi, A.H., Mishra, R.K., (2009) Acta Materialia, 57 (13), pp. 3683-3693.

[92] Papyrin, A., Kosarev, V., Klinkov, S., Alkhimov, A., Fomin, V., Cold Spray Technology. Amsterdam: Elsevier, 2007.

[93] Schmidt, T., Assadi, H., Gärtner, F., (2009) Journal of Thermal Spray Technology, 18 (5-6), pp. 794-808.

[94] Zou, Y., Qin, W., Irissou, E., et al. (2009) Scripta Materialia, 61 (9), pp. 899-902.

[95] Kobelev, N., Kolyvanov, E., Estrin, Y. (2008) Acta Materialia, 56 (7), pp. 1473-1481.

[96] Václavová, K., Stráský, J., Polyakova, V., et al. (2017) Materials Science and Engineering A, 682, pp. 220-228.

[97] Seiner, H., Sedlák, P., Bodnárová, L., et al. (2014) Key Engineering Materials, 606, pp. 87-90.

[98] Yin, S., Jenkins, R., Yan, X., et al. (2018) Materials Science and Engineering A, 734, pp. 67-76.

[99] Janovská, M., Minárik, P., Sedlák, P., et al. (2018) Journal of Materials Science, 53 (11), pp. 8545-8553.

[100] Jhang, K.-Y. Nonlinear ultrasonic techniques for non-destructive assessment of micro damage in material: A Review (2009) International Journal of Precision Engineering and Manufacturing, 10 (1), pp. 123-135.

[101] Yan, D., Neild, S.A., Drinkwater, B.W. (2012) NDT and E International, 47, pp. 18-25.

[102] Seiner, H., Sedlák, P., Straka, L., et al. (2016). In: Kainuma, R. (Ed.), Proceedings of ICFSMA'16, Tohoku University, Sendai, Japan.